Applied Materials Today 28 (2022) 101503

Contents lists available at ScienceDirect

Applied Materials Today

journal homepage: www.elsevier.com/locate/apmt

Evolution of the Seebeck effect in nanoparticle-percolated networks under applied strain

Yangyang Xin [a], Hussein Nesser [a], Jian Zhou [b], Gilles Lubineau [a,*]

[a] Mechanics of Composites for Energy and Mobility Lab, Mechanical Engineering Program, Physical Science and Engineering Division, King Abdullah University of Science and Technology (KAUST), Thuwal 23955-6900, Kingdom of Saudi Arabia

[b] School of Materials Science and Engineering, Sun Yat-sen University, Guangzhou 510275. Guangdong, PR China

ARTICLE INFO

Keywords:
Seebeck coefficient
Nanoparticles
Percolated networks
Stretchable temperature sensor

ABSTRACT

Nanoparticle clouds feature a unique evolution of the Seebeck coefficient under applied strain. At low strain, the Seebeck effect is very stable while, when a critical strain threshold is reached, it sharply decreases to zero. The evolution mechanism of this phenomenon that contributes to the development of various strain-insensitive sensors has yet to be documented. We elucidate here this evolution by proposing a phenomenological model supported by strong experimental evidence. We realize a full study of the Seebeck effect evolution for a network of nanoparticles under variable strain. We describe the evolution of this network as three subsequent stages: completely connected, partially connected, and disconnected. Based on the conductance-weighted formula, we theoretically analyze the evolution of the Seebeck coefficient in each stage. The Seebeck coefficient's initial stability is attributed to the connected pathways that exist in the first two stages. We validated these theoretical results by constructing percolated networks with embedded silver nanowires in elastomers and calculating the Seebeck coefficient under various stretching conditions. Finally, using the theoretical results as a guide, we created a temperature sensor that is highly resistant to mechanical damage.

1. INTRODUCTION

Owing to the increasing demand in the areas of soft robotics [1–3], wearable sensors in healthcare [4,5], and human/machine interfaces [6,7], the development of stretchable sensors, such as humidity [8–10], strain [11–13], pressure [14–16], and soft temperature sensors [17–19], has advanced considerably. Currently, most stretchable sensors employ resistance- or capacitance-based sensing techniques, where the microstructure of the functional layer of the sensor changes under various stimuli (mostly mechanical, thermal, or chemical stimuli). However, such microstructures are often affected by the applied strain; in other words, the measured signal depends on both the quantity being measured and the strain, affecting the accuracy of the obtained targeted information. For example, pyroelectric temperature, resistive temperature, and thermistor sensors do not return accurate information under stretching conditions because the applied strain modifies the conductance of the sensors' functional layers [20–25]. The Seebeck coefficient is highly insensitive to noise strain when compared to resistance and capacitance, and the related Seebeck effect has been widely applied to flexible/stretchable thermoelectric generators [26–28].

In our previous work, we designed a strain-insensitive stretchable temperature sensor based on the Seebeck effect of nanomaterial-percolated networks (i.e., silver (Ag) nanowires (NWs) and carbon nanotubes (CNTs)) [29]. The Seebeck coefficient was found to be very stable from zero strain to a high strain threshold (40%), above which it rapidly decreased to zero. The developed temperature sensor exhibited high linearity, strong repeatability, and considerable strain insensitivity, attributed to the excellent stability of the Seebeck coefficient below the strain threshold.

However, the underlying mechanisms of this unique evolution of the Seebeck coefficient under stretching conditions in clouds of nanoparticles is still not fully understood. To overcome this issue, we divided the problem into two subproblems: the structural evolution of nanoparticle-percolated networks under stretching conditions and the variation in the Seebeck coefficient related to the percolated network structure under different stretching conditions.

The first subproblem has been thoroughly investigated in the context of stretchable strain sensors [30–33]. In percolated networks, particles can be segregated into two groups: isolated particles that do not contribute to the percolation phenomena and particles connected to

* Corresponding author.
E-mail address: gilles.lubineau@kaust.edu.sa (G. Lubineau).

https://doi.org/10.1016/j.apmt.2022.101503
Received 24 February 2022; Received in revised form 19 April 2022; Accepted 27 April 2022
Available online 16 May 2022

percolated branches. The structure of percolated networks can be simplified from a net-like model to a model of parallelly connected bundles/pathways. These pathways consist of serially connected nanoparticles (or nanowires/nanotubes), and each pathway represents a percolated cluster of particles. All pathways are closed at the beginning of the stretching process because the nanoparticles are well connected. In the first stage, the equivalent length of the pathway increases because of the relative sliding among the connected nanoparticles under stretching. When the applied strain is increased further (stage 2), some nanoparticles lose contact, opening some pathways. Finally, all pathways are opened when the strain reaches the critical threshold in the last stage (stage 3) [30].

Several studies have examined the link between the Seebeck coefficient of particle clouds and their percolation properties; however, they did not consider the stretching condition [34–37]. A conductance-weighted formula has been established based on the conductance-weighted principle and the model of the parallelly connected pathways [34,36]. This formula describes the relation between the Seebeck coefficient of the global percolated networks and those of the substructures, i.e., the pathways.

Herein, to investigate the evolution of the Seebeck coefficient in percolated networks under stretching conditions, we conduct a theoretical analysis based on the structural evolution of percolated networks and conductance-weighted formula. Furthermore, we design experiments based on the percolated networks of AgNWs to validate the results of our theoretical analysis. The experimental results show good consistency with the theoretical results. Finally, we design a self-healing, damage-insensitive temperature sensor based on our theoretical analysis.

2. Experimental section

2.1. Materials

Two types of AgNWs were purchased from MilliporeSigma. The average length and diameter of the first kind of AgNW (hereinafter referred to as short AgNWs) were 10 μm and 60 nm, respectively. The average length and diameter of the second type of AgNW (hereinafter, referred to as long AgNWs) were 20–50 μm and 120 nm, respectively. Both types of AgNWs were dispersed in 0.5 wt.% isopropyl alcohol (IPA). The AgNW/IPA suspension was used directly without any change in its concentration. The short AgNWs were employed to prepare the samples for most experiments, whereas the long AgNWs were solely used to evaluate the stretchability of the percolated networks compared to that of the short AgNWs.

2.2. Ink printing on the polymeric nanofilter

A Microplotter II ink printer system (Sonoplot) was used to print inks of AgNWs in a straight line with a length of 25 mm on a polymeric nanofilter (Nuclepore polyester diameter: 35 mm), (Figure S1 (a)). To remove any aggregate that may block the nozzle during printing, the ink was passed through a syringe filter (Thermo Fisher Scientific; pore size: 30 μm) (Figure S1(b)). A commercial 27G syringe needle (inner diameter: 21 μm) was used as the printing nozzle. Before printing, the sharp tip was altered to a blunt tip using a sandpaper to provide a stable contact area between the ink droplets and the filter. The computer-controlled nozzle could move along the *X, Y* (working plan), and *Z* axes. The printing speed along the *X* and *Y* axes was fixed at 10 mm/s. A syringe pump was used to supply the ink at 30 μL/min. Printing timings were implemented to control the coverage of percolated networks. First, the ink was printed on a polymeric nanofilter using the printing system. Thereafter, IPA was rapidly removed via vacuum-assisted deposition (Figure S1 (c)), leaving only the nanomaterials of the ink before ink flushing, which increased the printing sharpness. After the vacuum-assisted deposition, the printed filter was dried in air for 10 min to remove any solvent residue, followed by washing three times with distilled water (Figure S1(d)).

2.3. Preparation of samples with percolated networks

First, polydimethylsiloxane (PDMS) and a curing agent were mixed at a weight ratio of 15:1, similar to the case in previous work [31]. Then, 5.3 g of the mixed PDMS was poured into a Petri dish to prepare the first layer. To remove air bubbles from PDMS, uncured PDMS was subjected to vacuum treatment for 15 min. Thereafter, the uncured PDMS was partially cured at 70 °C for 12 min to be in a viscous state. The printed nanofilter was transferred to the partially cured PDMS substrate by establishing a contact between the printed face of the nanofilter and the partially cured PDMS substrate (Figure S1(e)). The van der Waals forces ensured good adhesion between the printed nanofilter and the partially cured PDMS substrate. Thereafter, the PDMS substrate was heated in an oven at 80 °C for 10 min to complete the PDMS curing, affording an inlayed printed pattern on the substrate [31,38]. Next, the nanofilter was dissolved in dichloromethane (Figure S1(f)). The sample was connected to copper wires fixed to the substrate using Ag epoxy at the two ends of the percolated networks [31,38]. To protect the percolated networks, another 5.3 g of PDMS was poured on top of the sample, followed by vacuum and heat treatments at 80 °C for 1 h.

2.4. Characterizations

A Mechanical extension was controlled using a 5944 Instron machine (Figure S2(a)). A Keysight 34461A digital multimeter was employed to test the Seebeck voltage. The temperature difference between the two ends of the percolated networks was monitored using a picometer combined with two *K*-type thermocouples (Figure S2(b) and ((c)). The Seebeck coefficient was defined as $\alpha = V/\Delta T$, where V, and ΔT represent the Seebeck voltage, and temperature difference, respectively. The conductance of the percolated networks was tested using voltammetry resistance measurements ($G = I/V$, where G, V, and I represent the conductance, applied voltage, and current, respectively). The applied voltage was provided using an IT6720 DC power supply. The current and voltage were recorded using Keysight 34461A digital and Keysight 1242B multimeters, respectively.

Electrical conductance of the percolated networks under different applied voltages To verify the presence of electron tunneling and track the nonlinearities in the voltage/current relation, the conductance of the samples was analyzed under different applied voltages using voltammetry resistance measurements. The coverage of the nanomaterials was controlled in this section by printing 40 times. The coverage of the nanomaterials was controlled in this section by printing 40 times. The voltage was increased from 1 to 5 V using an IT6720 DC power supply. Moreover, different macroscopic strains were applied to the sample (0%–140%) during the measurement of the electrical conductance.

Seebeck coefficient of the percolated networks under different applied strains and temperature differences The sample used in this section has the same coverage (printing 40 times) as the previous section. First, we investigated the Seebeck coefficient of the printed percolated networks under different applied strains and temperature differences. Tests were conducted to obtain the evolution curves of the Seebeck coefficient as a function of the mechanical extension. In all the tests, the nominal strain was incrementally increased from 0% to the threshold, at which point the Seebeck voltage became zero. The step length between neighboring test points was 10% of the nominal strain, corresponding to a 1.5 mm extension using the Instron machine. Thereafter, to determine the influence of the temperature difference on the evolution curves namely, the change in the Seebeck coefficient with respect to the applied strain, the evolution curves were measured with temperature differences of 10 °C, 30 °C, and 60 °C.

Influence of the coverage on the Seebeck coefficient under different strains The influence of the coverage (density of the nanoparticles) on the

Seebeck coefficient under different strains was investigated. The coverage of the nanomaterials was controlled using different printing times (10, 20, and 80 times). Figure S3 shows the scanning electron microscopic (SEM) images of the samples with different coverage levels.

Influence of the morphology of the nanomaterials on the Seebeck coefficient under different strains The AgNW morphology was modified by controlling the AgNW length. Two different AgNW lengths were printed to form the percolated networks, and the evolution curves of the Seebeck coefficient based on these two networks were compared. Figure S4 presents the SEM images of the morphology of AgNWs with different lengths.

3. Results and discussion

3.1. Theoretical analysis

Herein, we aimed to design a simple predictive model that explains the evolution of both the global effective electrical conductance G and the global effective Seebeck coefficient α for a nanoparticle network under applied strain. Such a model can be kept relatively simple by making relevant assumptions on the network structure and its response to the growth of gaps at different junctions.

3.1.1. Conductance and Seebeck coefficient of a nanoparticle network

First, we simplified the nanoparticle network (Fig. 1(a)) into parallelly connected pathways (Fig. 1(b)). Based on the previous studies about the morphology of the nanoparticle-percolated networks, the nanoparticles can be organized into different families: (a) isolated particles; (b) particles belonging to "dead-ends" in the percolated clusters that do not participate in conduction; and (c) particles within the functional parts or percolated clusters, which contribute to macroscopic conduction [32,33]. Considering that there is a finite number of distinct conductive pathways, a conductance-weighted model is introduced as a surrogate model to bridge G and α (the properties of the entire nanoparticle network) to the properties of different pathways (G_j and α_j represent the electrical conductance and Seebeck coefficient of the jth pathway, respectively) [37,39]. Assume that I and V denote the global current and voltage between the two ends of the nanoparticle network, respectively, and I_j and V_j denote the current through the jth pathway and the voltage between the two ends of the jth pathway, respectively. Then, the following relations describe the generation of voltage between the ends of the network based on a combination of Ohmic and Seebeck effects:

$$V = I/G + \alpha\Delta T, \qquad V_j = I_j/G_j + \alpha_j\Delta T. \tag{1}$$

Considering the parallel connection of the pathways, it is evident that

$$I = \sum_1^n I_j, \qquad V = V_j, \tag{2}$$

where n denotes the number of active pathways for a given morphology of the network. Combining Eqs. (1) and (2), we achieve

$$G = \sum_1^n G_j, \qquad \alpha = \frac{\sum_1^n \alpha_j G_j}{\sum_1^n G_j}. \tag{3}$$

If α_j and G_j are known, α and G can be estimated easily using the conductance-weighted formula described in Eq. (3).

Eq. (3) presents a crucial feature of nanoparticle networks: the conductance'not the Seebeck coefficient'is highly dependent on the number of conductive paths. To illustrate this point, assume, for example, an extreme configuration where all pathways exhibit similar properties, i.e., the same conductance values and Seebeck coefficient ($G_i = G_j = G_0$ and $\alpha_i = \alpha_j = \alpha_0$, $\forall(i,j)$). In this case, we achieve $G = nG_0$ and $\alpha = \alpha_0$. This implies that if the pathways progressively disconnect (n is decreasing), the electrical conductance will also decrease accordingly, while the Seebeck coefficient will remain constant until the last pathway has been disconnected.

Modeling outcome: We expect a progressive decrease in the electrical conductance during stretching. Alternatively, the Seebeck coefficient is expected to remain constant until it sharply drops from its nominal value to zero above the stretch threshold called the "Seebeck extinction stretch threshold", which corresponds to the electrical disconnection of the last pathway.

We validate this theoretical prediction in the following theoretical analysis and experimental verification sections.

3.1.2. Evolution of the pathway properties (G_j, α_j) with mechanical/thermal loading

In the previous section, we elucidated the relation between the global properties of the nanoparticle network and the properties of each pathway (G_j, α_j). Next, to understand the evolution of each pathway (G_j, α_j), we must examine the electron transfer induced either by an external power source (conductance part) or temperature (Seebeck part).

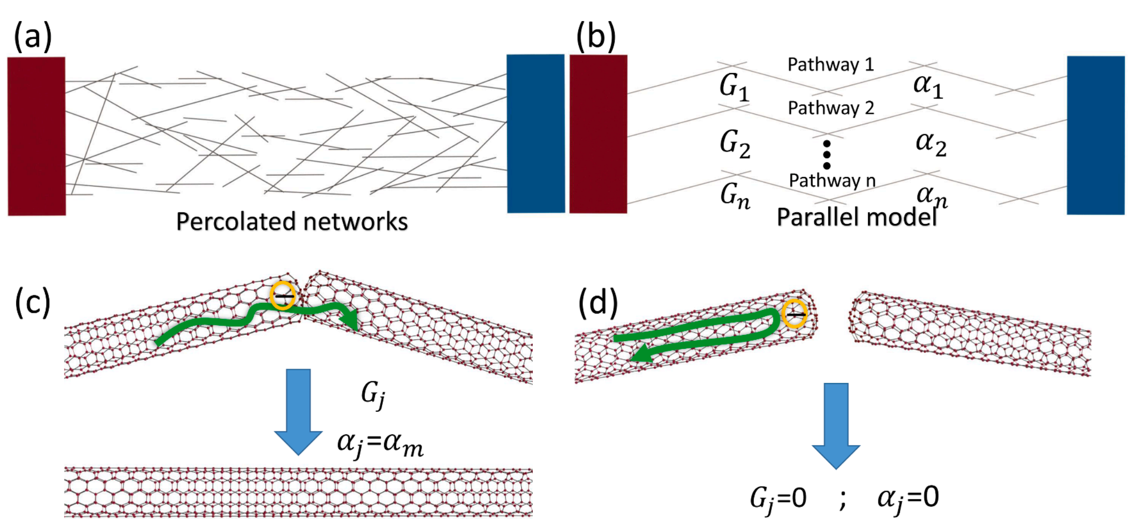

Fig. 1. Simplification of the percolated networks and their structural evolution under applied strain. (a) Schematics of the percolated networks. (b) Simplification of the percolation networks as a set of pathways in parallel. (c) and (d) Relative conductance and Seebeck coefficient for the completely connected and disconnected pathways, respectively.

Regarding the Seebeck effect, the potential energy of the electrons on the hot side increases considerably, higher than that on the cold side, driving electrons to the cold side. The resulting accumulation of electrons on the cold side induces a Seebeck voltage V_T. Regarding the electrical conductance, a potential difference between both the sides is generated using an external power source. These mechanisms, as well as the corresponding values of α_j and G_j, can be described using Eq. (4):

$$G_j = \frac{I_P}{V_P} \quad ; \quad \alpha_j = \frac{V_T}{T_h - T_c}, \tag{4}$$

where T_h and T_c represent the temperatures of the hot and cold sides, respectively, V_T is the related Seebeck voltage, and the I_P represents the current flowing through the pathway induced by an applied voltage V_P.

For completely connected nanoparticles, the electrons can easily transfer through the junction. Thus, the pathway for the completely connected nanoparticles can be regarded as a single long nanowire (Fig. 1(c)) with the same Seebeck coefficient as the material (α_m):

$$\alpha_j = \alpha_m. \tag{5}$$

When a gap is created between two NWs, it is difficult for electrons to pass through the gap, inducing a zero current because of a relatively high energy barrier (Fig. 1(d)). Therefore, we assume that the Seebeck coefficient and conductance for the disconnected pathway decrease to zero:

$$\alpha_j = 0; \qquad G_j = 0. \tag{6}$$

Reality is, in fact, more complex as tunneling is voltage-dependent and might still be activated by ultra-high voltages locally. But the above binary assumption is enough to demonstrate our point about the evolution of the network.

3.1.3. Predicted overall evolution of the conductance and Seebeck coefficient

In summary, Fig. 2(a) shows a simplified model with three proposed configurations of the nanoparticle network under applied strain [30,31].

In regime 1, all the pathways are well-percolated and most junctions are in contact, with no gaps. Thus, the conductance of each pathway decreases only slightly due to the equivalent elongation caused by stretching. Conversely, the Seebeck coefficient of the pathways are all equal to α_m because no gap exists. Combining the aforementioned analysis with the conductance-weighted model, the conductance of the nanoparticle network is determined to be high and relatively insensitive to the stretch; further, the Seebeck coefficient is equal to the Seebeck coefficient of the nanoparticles and is constant in regime 1 (Fig. 2(b)).

In regime 2, the pathways are partially connected and some gaps begin to appear, inducing a rapid decrease in the conductance of the percolated networks (Fig. 2(b)). The disconnected pathways do not notably affect the Seebeck coefficient. To verify this conclusion, we assume that the first h pathways are completely connected with a Seebeck coefficient of α_m, and $h+1$ to n pathways are disconnected with a Seebeck coefficient of zero. Applying this assumption to the conductance-weighted formula, we obtain

$$\alpha = \frac{\sum_1^h \alpha_m G_j}{\sum_1^h G_j} = \alpha_m. \tag{7}$$

In regime 3, all pathways are disconnected because of the large applied strain. The conductance progressively decreases to zero. As no completely connected pathway remains, the Seebeck coefficient decreases sharply from its nominal value to zero (Fig. 2(b)).

Our qualitative modeling also provides some indications on the evolution of the response with respect to the coverage (Figure S5(a)) and (the morphology of the nanoparticles (Figure S5(b)). With increasing coverage, the range of regime 2 is expected to increase as the disconnection of the last pathway is delayed. This should increase the stability domain of the Seebeck coefficient, described by the Seebeck extinction threshold. Next, we estimated the influence of the nanoparticle morphology (length) on the Seebeck coefficient. A similar trend is observed when long nanoparticles are used instead of short nanoparticles. Long nanoparticles can ensure contact under large stretching and induce the extension of regimes 1 and 2. Accordingly, using long nanoparticles, we can extend the stage at which the Seebeck coefficient remains stable.

3.2. Experimental verification

We designed experiments to verify the results of the above-described theoretical analysis.

3.2.1. Evolution of the conductance of the network

First, we monitored the evolution of the conductance of a sample with increasing strain under different applied voltages.

Fig. 3 (a) shows that the conductance decreases with the applied strain, consistent with our theoretical prediction. Moreover, the conductance is sensitive to the applied voltage when the stretch becomes very high (>90%), attributed to electron tunneling. This electron tunneling effect has been reported in nanomaterial-based percolated networks and was investigated in our previous work [31]. The conductance shows a positive relation with the applied voltage because a high voltage can cause additional electrons to tunnel through the gap [40].

At low strain (regime 1), the conductance is insensitive to the applied voltage (Fig. 3(a)). The transfer of charge is guided by the direct contact between the particles that overlap widely. Tunneling may exist;

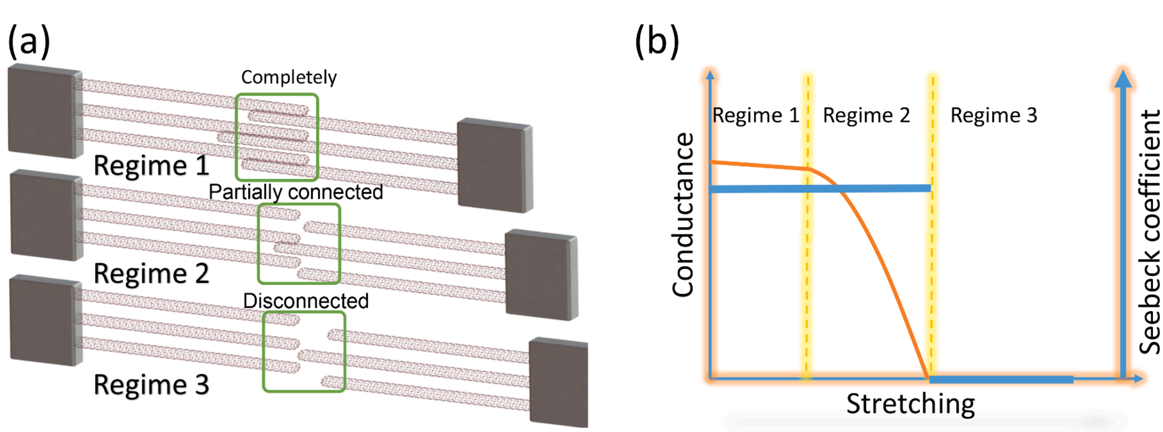

Fig. 2. Investigation of conductance and the Seebeck coefficient under different stretching conditions. (a) Three-regime assumption of percolated networks under applied strain. (b) Illustration of the expected conductance and Seebeck coefficient in each regime.

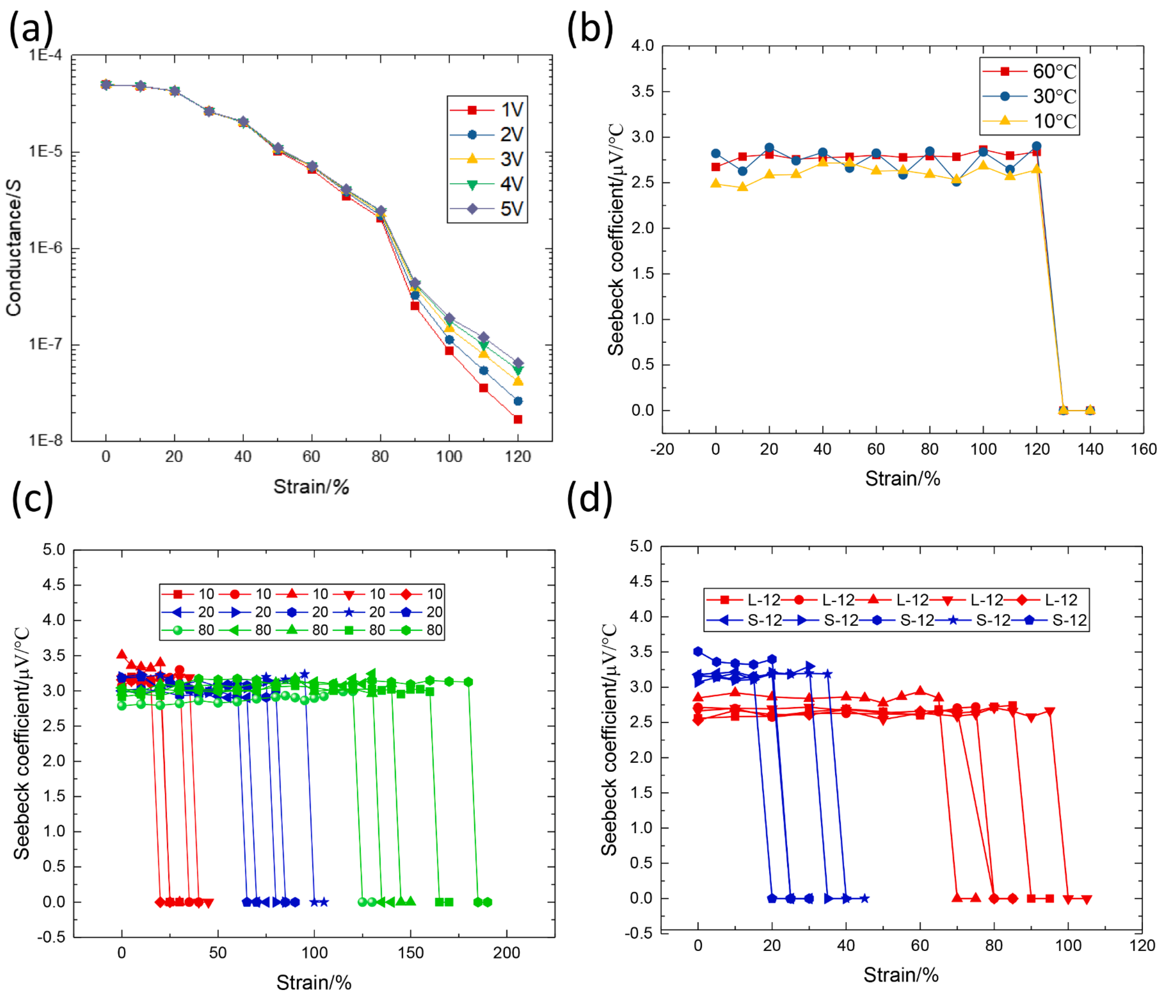

Fig. 3. Experimental results of the electrical conductance and Seebeck coefficient of the percolated networks under stretching. (a) Conductance of the percolated networks under stretching at different applied voltages, showing voltage-dependent conductance. (b) Changes in the Seebeck coefficient changes with respect to the strain with different temperature differences, showing two-stage properties and insensitivity to temperature difference. (c) Seebeck coefficient at different coverage levels under applied strain, indicating that a large coverage can increase the extent of the stable stage. (d) Seebeck coefficient evolution curves with different AgNW lengths, showing that long nanowires can enhance the stability range.

however, it is very limited. The conductance curves overlap until a 30% strain is achieved, above which they begin to deviate from each other. This indicates that "regime 1" is applicable until 30% strain, above which other mechanisms become applicable.

Above 30% strain, the conductance becomes sensitive to the applied voltage and exhibits an increasing trend as the voltage increases (Fig. 3(a)). This voltage-sensitivity of the conductance is observed from 30% strain, although it becomes predominant above 90% strain. This voltage-sensitive behavior can be explained by following effects: (a) the high stretch induces to a gradual increase in the gap at most junctions and (b) as the tunneling becomes a major mechanism in these junctions with a gap, a high applied voltage induces sufficient potential energy for the electrons to tunnel through the junctions.

This first series of results (Fig. 3(a)) illustrates what is classically known about voltage-dependent and strain-dependent conductance in nanoparticle-percolated networks: the progressive multiplication of junctions with a gap and the increasing influence of tunneling under applied strain.

3.2.2. Evolution of the Seebeck coefficient

Second, we measured the Seebeck coefficient with temperature differences of 10 °C, 30 °C, and 60 °C under different applied strains (Fig. 3(b)). The Seebeck coefficient is very stable and independent of the stretching level until a strain of 120%, above which it suddenly drops to zero. This is consistent with our theoretical results, which demonstrates that as long as at least one of the pathways is still completely connected, the Seebeck effect is not affected by the progressive disconnection of some pathways. When the last conductive pathway is disconnected, the Seebeck coefficient suddenly drops to zero, as explained previously. Note that this threshold is almost independent of the temperature differences: for 10 °C, 30 °C, or 60 °C, the Seebeck coefficient drops to zero around the same 120% strain threshold. This is because, compared with the applied voltage (>1 V) in the conductance analysis, the relatively low Seebeck voltage (approximately 25 μV and 150 μV for temperature difference of 10 °C and 60 °C, respectively) could not support electron tunneling.

Next, we estimate the Seebeck coefficient of percolated networks with different coverage levels (i.e., the density of particles per unit area) under stretching; the results are shown in Fig. 3(c). We control the coverage using the printing times. Moreover, we examine three coverage levels and test five samples for each level. The reproducibility is found to be very good from sample to sample, and the threshold at which the Seebeck coefficient drops to zero is highly dependent on the coverage (Fig. 3(c)). The Seebeck coefficient is stable in a wide strain range at a high coverage level because the number of completely connected pathways increases, consistent with our theoretical results.

Finally, we analyze the influence of the morphology of the nanomaterials on the Seebeck coefficient of percolated networks printed using different AgNW lengths; the results are shown in Fig. 3(d). The mean value of the strain threshold of the Seebeck coefficient for the long AgNWs is 85%, while it is approximately 30% for the short AgNWs (10 μm). This result is also consistent with our theoretical result because the pathways in networks with long AgNWs exhibit extended regimes 1 and 2; the disconnection of the last conductive pathway occurs considerably later in the case of the long AgNWs.

3.3. Self-healing temperature sensing application

Here, we exploit the obtained theoretical understanding to design a self-healing temperature sensor. Notably, the Seebeck effect appears almost insensitive to network perturbations as long as at least one conductive pathway is still active. This indicates that the Seebeck effect can be restored in damaged nanonetworks by restoring a limited number of conductive pathways, enabling easy self-healing.

First, we print a "U"-shaped temperature-sensing layer comprising single-wall CNTs (SWCNTs) and AgNWs on a nanofilter, as described in our previous paper [29]. Thereafter, the printed percolated networks are transferred and embedded on a PDMS substrate to form the functional layer of the self-healing temperature sensor (Fig. 4(a)). The second and fourth layers comprise patterned PDMS substrates, forming two separate chambers when the four layers overlap and are glued together. We employ a CO_2 laser machine to engrave poly(methyl methacrylate) (PMMA) as the model (Figure S6). Fig. 4(b) shows the patterned substrate fabricated using the laser-engraved PMMA model. The four layers are glued together, and their surfaces are spin-coated using the uncured PDMS, followed by 2 h of heating at 80 °C. Thereafter, the two chambers are filled, one with pure PDMS and the other with the curing agent (Fig. 4(c)).

Second, after fabricating the self-healing temperature sensor, we cut the SWCNT line (Fig. 4(d)). The injected liquid leaks out of the designed chambers, after which the sensor is released and cured at room temperature for 24 h. Fig. 4(e) shows the temperature sensor after self-healing. To examine the mechanical integrity of the substrate after self-healing, we bent the sample (Fig. 4(f)). We investigate the conductance and Seebeck effect of the temperature sensor before and after the cutting and self-healing processes (Fig. 4(g) and (h)). The conductance decreases by approximately two-thirds after cutting. This was expected because the conductance is highly dependent on the number of percolated pathways that cannot be completely recovered with no disconnections during self-healing. However, the I/V curve retain good linearity, indicating the presence of many completely connected pathways in the percolated networks after self-healing. Unlike the conductance, the evolution curve of the Seebeck voltage with respect to the temperature difference remains nearly unchanged before and after the cutting and self-healing processes. Therefore, the Seebeck coefficient of this self-healing temperature sensor is insensitive to mechanical damage such as cutting.

This demonstration opens new paths when it comes to the design of stable sensors that can be insensitive to mechanical damage. It also indicates that the Seebeck effect is globally very independent of the variations in microstructures, that is also a path to make such sensors relatively independent on processing quality and conditions.

4. Conclusions

In summary, based on the conductance-weighted model and the

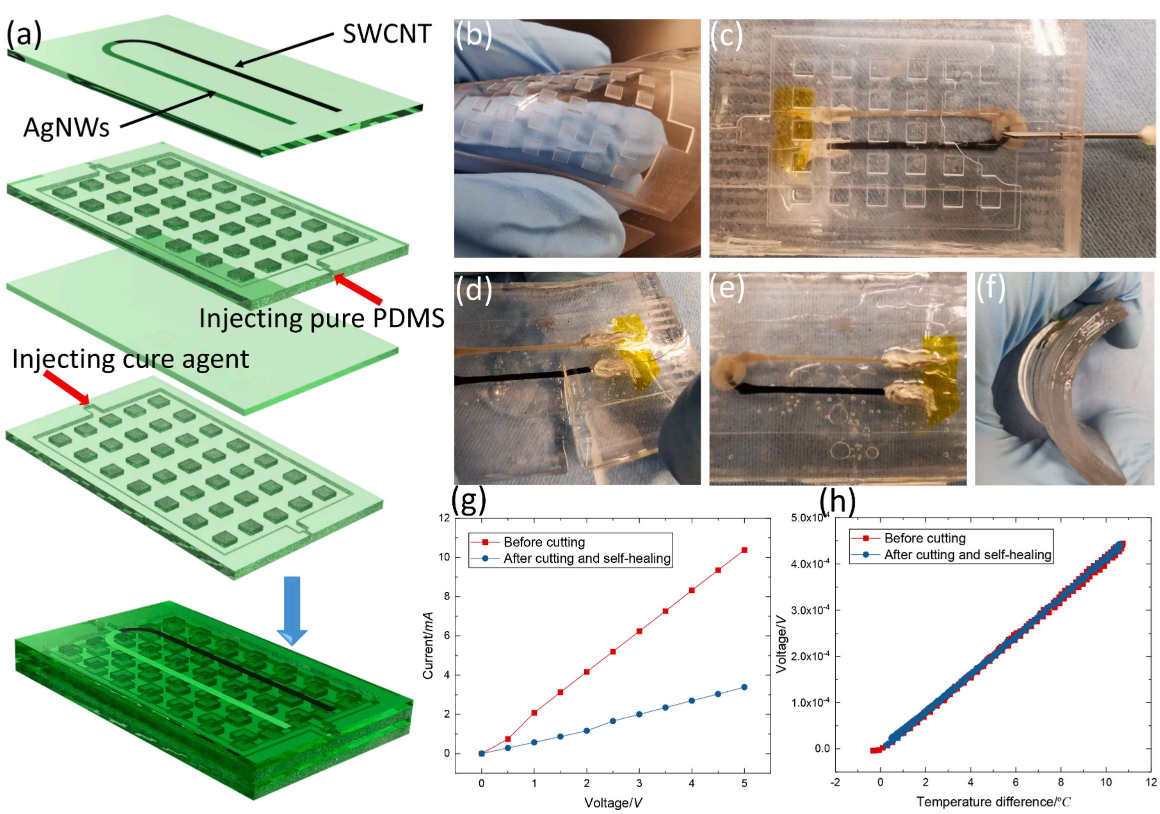

Fig. 4. Self-healing temperature sensor based on the Seebeck coefficient, comprising percolated networks of single-wall CNTs (SWCNTs) and AgNWs. (a) Structure of the self-healing temperature sensor containing two chambers to space out the pure PDMS and the curing agent. (b) Image of the patterned PDMS substrate used to form the chamber. (c) Injection of pure PDMS or curing agent into the chambers using a syringe. (d) Cutting the temperature sensor to induce the leakage of the liquid PDMS and curing agent. (e) Image of the temperature sensor after self-healing. (f) Temperature sensor bending after the cutting and self-healing processes. (g) I/V curves of the temperature sensor before and after cutting and self-healing processes, showing a decrease in the conductance of the percolated networks. (h) Change in the Seebeck voltage with respect to the temperature difference before and after cutting and self-healing processes, indicating almost no change in the performance of the temperature sensor.

evolution of percolated networks under stretching conditions, we conducted a theoretical analysis to explain the evolutionary characteristics of the Seebeck coefficient of percolated networks under different applied strains. We found that the stability of the Seebeck coefficient under low strain is attributed to the completely connected pathways present in regimes 1 and 2. Moreover, we demonstrated that the threshold of the Seebeck coefficient is independent of the temperature difference. Although the conductance of the percolated network progressively decreases under stretching because of the partial disconnection of the nanoparticle pathways (i.e., the classic piezoresistive effect usually employed in the design of many sensors), the Seebeck coefficient remains constant as long as at least one percolated pathway exists in the structure. Long NWs and a high coverage can increase the duration of the stable Seebeck coefficient stage. These theoretical results were supported by experimental results, suggesting that the theoretical analysis successfully revealed the evolution mechanism of the Seebeck coefficient under stretching conditions. Finally, we implemented this theoretical results to develop a self-healing temperature sensor that was insensitive to mechanical damage.

Data availability

The datasets generated during and/or analyzed during the current study are available from the corresponding author on reasonable request.

CRediT authorship contribution statement

Yangyang Xin: Conceptualization, Supervision, Investigation, Data curation, Formal analysis, Writing – review & editing. **Hussein Nesser:** Writing – review & editing. **Jian Zhou:** Conceptualization, Supervision. **Gilles Lubineau:** Conceptualization, Supervision, Data curation, Formal analysis, Writing – review & editing.

Declaration of Competing Interest

The authors declare that they have no known competing financial interests or personal relationships that could have appeared to influence the work reported in this paper.

Acknowledgments

The research reported herein was supported by King Abdullah University of Science and Technology (KAUST), under award number BAS/1/1315-01-01. The authors thank Ragesh Chellattoan for helping with the SEM images and Saad Nauman for his input on the fabrication method for the self-healing substrate.

Supplementary material

Supporting Information: Sample preparation and characterization as well as additional results of theoretical analysis are presented in the Supporting Information.

Supplementary material associated with this article can be found, in the online version, at doi:10.1016/j.apmt.2022.101503.

References

[1] Y. Cheng, R. Wang, J. Sun, L. Gao, A stretchable and highly sensitive grphene-based fiber for sensing tensile strain, bending, and torsion, Adv. Mater. 27 (45) (2015) 7365–7371.
[2] J. Zhou, H. Yu, X. Xu, F. Han, G. Lubineau, Ultrasensitive, stretchable strain sensors based on fragmented carbon nanotube papers, ACS Appl. Mater. Interfaces 9 (5) (2017) 4835–4842.
[3] J. Zhou, X. Xu, Y. Xin, G. Lubineau, Coaxial thermoplastic elastomer-wrapped carbon nanotube fibers for deformable and wearable strain sensors, Adv. Funct. Mater. 28 (16) (2018) 1705591.
[4] C. Zhu, A. Chortos, Wang, Stretchable temperature-sensing circuits with strain suppression based on carbon nanotube transistors, Nat. Electron. 1 (3) (2018) 183.
[5] J. Kim, M. Lee, H.J. Shim, Ghaffari, Stretchable silicon nanoribbon electronics for skin prosthesis, Nat. Commun. 5 (2014) 5747.
[6] S. Lee, Y. Inoue, Kim, A strain-absorbing design for tissue–machine interfaces using a tunable adhesive gel, Nat. Commun. 5 (2014) 5898.
[7] S.R. Soekadar, M. Witkowski, C. Gómez, Hybrid EEG/EOG-based brain/neural hand exoskeleton restores fully independent daily living activities after quadriplegia, Sci. Robot. 1 (1) (2016) 32–96.
[8] T.Q. Trung, Ramasundaram, Transparent, stretchable, and rapid-response humidity sensor for body-attachable wearable electronics, Nano Res. 10 (6) (2017) 2021–2033.
[9] G. Zhou, J.-H. Byun, Oh, Highly sensitive wearable textile-based humidity sensor made of high-strength, single-walled carbon nanotube/poly (vinyl alcohol) filaments, ACS Appl. Mater. Interfaces 9 (5) (2017) 4788–4797.
[10] Y. Pang, J. Jian, Tu, Wearable humidity sensor based on porous graphene network for respiration monitoring, Biosens. Bioelectron. 116 (2018) 123–129.
[11] X. Wu, C. Lu, Y. Han, Z. Zhou, G. Yuan, X. Zhang, Cellulose nanowhisker modulated 3D hierarchical conductive structure of carbon black/natural rubber nanocomposites for liquid and strain sensing application, Compos. Sci. Technol. 124 (2016) 44–51.
[12] J. Zhou, X. Xu, Y. Hu, G. Lubineau, Deformable and wearable carbon nanotube microwire-based sensors for ultrasensitive monitoring of strain, pressure and torsion, Nanoscale 9 (2017) 604–612.
[13] M. Amjadi, A. Pichitpajongkit, S. Lee, S. Ryu, I. Park, Highly stretchable and sensitive strain sensor based on silver nanowire–elastomer nanocomposite, ACS Nano 8 (5) (2014) 5154–5163.
[14] S. Lee, A. Reuveny, Reeder, A transparent bending-insensitive pressure sensor, Nat. Nanotechnol. 11 (5) (2016) 472.
[15] J. Lee, H. Kwon, Seo, Conductive fiber-based ultrasensitive textile pressure sensor for wearable electronics, Adv. Mater. 27 (15) (2015) 2433–2439.
[16] Y. Gao, H. Ota, Schaler, Wearable microfluidic diaphragm pressure sensor for health and tactile touch monitoring, Adv. Mater. 29 (39) (2017) 1701985.
[17] H. Yang, D. Qi, Liu, Soft thermal sensor with mechanical adaptability, Adv. Mater. 28 (41) (2016) 9175–9181.
[18] S.Y. Hong, Y.H. Lee, Park, Stretchable active matrix temperature sensor array of polyaniline nanofibers for electronic skin, Adv. Mater. 28 (5) (2016) 930–935.
[19] M. Cai, S. Nie, Y. Du, C. Wang, J. Song, Soft elastomers with programmable stiffness as strain-isolating substrates for stretchable electronics, ACS Appl. Mater. Interfaces 11 (15) (2019) 14340–14346.
[20] M. Jung, K. Kim, B. Kim, H. Cheong, K. Shin, O. Kwon, J. Park, S. Jeon, Paper-based bimodal sensor for electronic skin applications, ACS Appl. Mater. Interfaces 9 (2017) 26974–26982.
[21] T. Someya, Y. Kato, T. Sekitani, S. Iba, Y. Noguchi, Y. Murase, H. Kawaguchi, T. Sakurai, Conformable, flexible, large-area networks of pressure and thermal sensors with organic transistor active matrixes, Proc. Natl. Acad. Sci. 102 (35) (2005) 12321–12325.
[22] S.K. Mahadeva, S. Yun, J. Kim, Flexible humidity and temperature sensor based on cellulose–polypyrrole nanocomposite, Sens. Actuators, A 165 (2) (2011) 194–199.
[23] S. Harada, K. Kanao, Y. Yamamoto, T. Arie, S. Akita, K. Takei, Fully printed flexible fingerprint-like three-axis tactile and slip force and temperature sensors for artificial skin, ACS Nano 8 (12) (2014) 12851–12857.
[24] K. Kanao, S. Harada, Y. Yamamoto, W. Honda, T. Arie, S. Akita, K. Takei, Highly selective flexible tactile strain and temperature sensors against substrate bending for an artificial skin, RSC Adv. 5 (38) (2015) 30170–30174.
[25] Y. Khan, A.E. Ostfeld, C.M. Lochner, A. Pierre, A.C. Arias, Monitoring of vital signs with flexible and wearable medical devices, Adv. Mater. 28 (22) (2016) 4373–4395.
[26] S. Xu, M. Hong, X. Shi, M. Li, Q. Sun, Q. Chen, M. Dargusch, J. Zou, Z.-G. Chen, Computation-guided design of high-performance flexible thermoelectric modules for sunlight-to-electricity conversion, Energy Environ. Sci. 13 (10) (2020) 3480–3488.
[27] X.-L. Shi, W.-Y. Chen, T. Zhang, J. Zou, Z.-G. Chen, Fiber-based thermoelectrics for solid, portable, and wearable electronics, Energy Environ. Sci. 14 (2) (2021) 729–764.
[28] L. Liang, H. Lv, X.-L. Shi, Z. Liu, G. Chen, Z.-G. Chen, G. Sun, A flexible quasi-solid-state thermoelectrochemical cell with high stretchability as an energy-autonomous strain sensor, Mater. Horiz. 8 (10) (2021) 2750–2760.
[29] Y. Xin, J. Zhou, G. Lubineau, A highly stretchable strain-insensitive temperature sensor exploits the seebeck effect in nanoparticle-based printed circuits, J. Mater. Chem. A 7 (42) (2019) 24493–24501.
[30] J. Zhou, H. Yu, X. Xu, F. Han, G. Lubineau, Ultrasensitive, stretchable strain sensors based on fragmented carbon nanotube papers, ACS Appl. Mater. Interfaces 9 (5) (2017) 4835–4842.
[31] Y. Xin, J. Zhou, X. Xu, G. Lubineau, Laser-engraved carbon nanotube paper for instilling high sensitivity, high stretchability, and high linearity in strain sensors, Nanoscale 9 (30) (2017) 10897–10905.
[32] G. Lubineau, A. Mora, F. Han, I. Odeh, R. Yaldiz, A morphological investigation of conductive networks in polymers loaded with carbon nanotubes, Comput. Mater. Sci 130 (2017) 21–38.
[33] A. Mora, F. Han, G. Lubineau, Estimating and understanding the efficiency of nanoparticles in enhancing the conductivity of carbon nanotube/polymer composites, Results Phys. 10 (2018) 81–90.
[34] M. Piao, M.-K. Joo, J. Na, Y.-J. Kim, M. Mouis, G. Ghibaudo, S. Roth, W.-Y. Kim, H.-K. Jang, G.P. Kennedy, et al., Effect of intertube junctions on the thermoelectric

power of monodispersed single walled carbon nanotube networks, J. Phys. Chem. C 118 (46) (2014) 26454–26461.
[35] Y. Nakai, K. Honda, K. Yanagi, H. Kataura, T. Kato, T. Yamamoto, Y. Maniwa, Giant seebeck coefficient in semiconducting single-wall carbon nanotube film, Appl. Phys Express 7 (2) (2014) 025103.
[36] M. Baxendale, K. Lim, G. Amaratunga, Thermoelectric power of aligned and randomly oriented carbon nanotubes, Phys. Rev. B 61 (19) (2000) 12705.
[37] H. Romero, G. Sumanasekera, G. Mahan, P. Eklund, Thermoelectric power of single-walled carbon nanotube films, Phys. Rev. B 65 (20) (2002) 205410.
[38] Y. Xin, J. Zhou, R. Tao, X. Xu, G. Lubineau, Making a bilateral compression/tension sensor by pre-stretching open-crack networks in carbon nanotube papers, ACS Appl. Mater. Interfaces 10 (39) (2018) 33507–33515.
[39] K. Esfarjani, M. Zebarjadi, Y. Kawazoe, Thermoelectric properties of a nanocontact made of two-capped single-wall carbon nanotubes calculated within the tight-binding approximation, Phys. Rev. B 73 (8) (2006) 085406.
[40] K.-H. Müller, M. Yajadda, Electron transport in discontinuous gold films and the effect of coulomb blockade and percolation, J. Appl. Phys. 111 (12) (2012) 123705.